IET Microwaves, Antennas & Propagation

Research Article

Electrically varactor-tuned bandpass filter with constant bandwidth and self-adaptive transmission zeros

ISSN 1751-8725
Received on 21st October 2016
Revised 4th May 2017
Accepted on 25th May 2017
E-First on 7th August 2017
doi: 10.1049/iet-map.2016.0919
www.ietdl.org

Jing Cai[1], Jian-Xin Chen[1] ✉, Xue-Feng Zhang[1], Yong-Jie Yang[1], Zhi-Hua Bao[1]
[1]School of Electronics and Information, Nantong University, 9 Seyuan Road, Nantong 226019, Jiangsu, People's Republic of China
✉ *E-mail: jjxchen@hotmail.com*

Abstract: This paper presents a wideband frequency-agile bandpass filter (BPF) with constant absolute bandwidth (ABW) and two self-adaptive transmission zeros (TZs) at lower and higher stopbands. A frequency-dependent source-to-load (S-L) coupling is incorporated in this design so that two symmetrical TZs close to the tunable passband are self-adaptive and the separations between the passband center frequency and two TZs can almost keep the same for achieving continuous high selectivity in the frequency-tuning process. A lumped capacitor C_1 and a varactor diode are loaded to the two open ends of the half-wavelength resonator. With the aid of the employed C_1, the desired external quality factor can be obtained in a wide frequency-tuning range. Meanwhile, properly choosing the specific coupling region can make the coupling coefficient close to the desired one. As a result, the constant ABW can be obtained as the passband frequency changes. For demonstration, the proposed BPF is designed and fabricated. The simulated and measured results are presented. The results exhibit the tuning range from 430 MHz to 720 MHz with 3-dB constant ABW of around 75 MHz and the insertion loss of 1.34–2.92 dB, and the distance from TZs to center frequency is nearly constant at 150 MHz.

1 Introduction

Reconfigurable/tunable microwave devices are highly demanded in modern wireless communication systems. To cater for this trend, microwave filter, as a key frequency-selective component in the system, should be reconfigurable or tunable, which has been a hot research topic in the academic and industrial circles. In the past decades, various kinds of tunable filters have been developed using radio-frequency (RF) microelectromechanical system [1–3], yttrium–iron–garnet [4], piezoelectric transducer [5], semiconductor diodes, and so on. In among, varactor-tuned bandpass filters (BPFs) are widely explored and applied due to their small size, rapid tuning speed, and low cost [6–20]. Accordingly, many efforts have been paid to make the tunable BPFs more attractive such as expanding the frequency-tuning range, improving the linearity of the BPFs and realising controllable bandwidth [16–20].

It is well known that the selectivity is a key performance of the filter. For a frequency-tuning filter, the performance of the filter usually varies as the passband frequency is changed including the passband width and selectivity. Recently, the designs with constant absolute bandwidth (ABW)/fractional bandwidth have drawn much attention of the microwave engineer. However, the selectivity has rarely mentioned in these previous designs. For example, the tunable filters in [21–23] have only one or none transmission zero (TZ). In [24, 25], two or more TZs in the stopbands are realised, but the passband selectivity is variable in the frequency-tuning process. To achieve the continuous high selectivity, which is highly desirable in the tunable filter, a tunable source-to-load (S–L) coupling realised by extra varactor diodes in [26] is used to generate two TZs, and the TZs are always close to the passband. However, too many varactor diodes are used, leading to the increase of IL (about 3.8–4.9 dB).

In this paper, a high-selectivity tunable BPF with two self-adaptive TZs and constant ABW is presented. A frequency-dependent S–L coupling is incorporated for the first time to realise two self-adaptive TZs symmetrically loaded at the two sides of the passband. The two TZs keep the same distance to the passband centre frequency, so that continuously high selectivity can be kept as the passband frequency changes, which is highly desirable in many practical applications. Meanwhile, both the desired external quality factor (Q_e) and the coupling coefficient (K_{12}) between resonators in a wide-frequency-tuning range can be obtained by choosing the proper parameters. As a result, the constant ABW of the proposed tunable filter, which could hardly be affected by the S–L coupling, can be obtained as the passband frequency varies. The demonstration tunable filter is designed and implemented, and the simulated and measured results are presented, showing good agreement.

2 Design considerations for the proposed tunable BPF

The schematic layout of the proposed second-order tunable BPF with its coupling mechanism is illustrated in Fig. 1. It consists of two coupled asymmetric half-wavelength ($\lambda/2$) resonators with varactor C_v and capacitor C_1 loaded at both ends, a pair of feeding lines through capacitor C_2 as shown in Fig. 2 and two shunt stubs for realising S–L coupling. The specifications of the proposed second-order tunable BPF with Chebyshev response are ABW = 75 MHz and two TZs located at $f_0 \pm 150$ MHz, where f_0 is the centre frequency of the tunable passband. The filter design depends on extracting K_{12} and Q_e, and the synthesis of the self-adaptive TZs is based on the coupling matrix [$\boldsymbol{M}$] shown below

$$\boldsymbol{M} = \begin{array}{c} \\ S \\ 1 \\ 2 \\ L \end{array} \begin{array}{c} \begin{array}{cccc} S & 1 & 2 & L \end{array} \\ \begin{bmatrix} 0 & M_{S1} & 0 & -M_{SL} \\ M_{S1} & 0 & M_{12} & 0 \\ 0 & M_{12} & 0 & M_{2L} \\ -M_{SL} & 0 & M_{2L} & 0 \end{bmatrix} \end{array} \quad (1a)$$

$$K_{12} = \frac{A}{f_0} \times M_{12} \quad (1b)$$

$$Q_e = \frac{f_0}{A \times M_{S1}^2} = \frac{f_0}{A \times M_{2L}^2} \quad (1c)$$

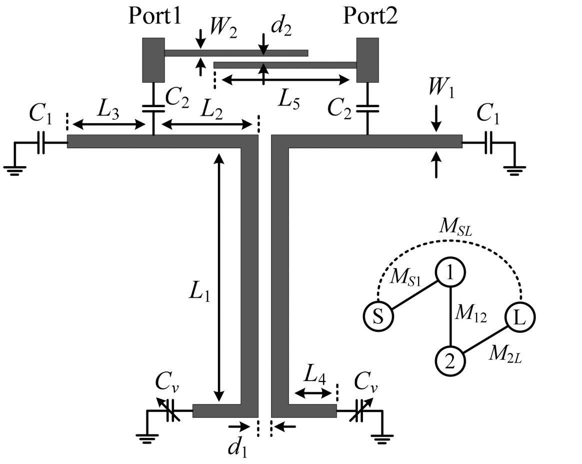

Fig. 1 *Layout of the proposed tunable BPF with constant ABW and its coupling mechanism*

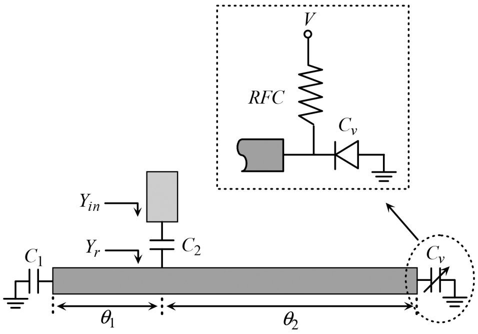

Fig. 2 *Feeding scheme for the resonator with the implementation of the tunable capacitor C_v, where the radio frequency choke (RFC) means the RF choke realised by a resistor with a large value of 51 kΩ*

where A represents ABW. The required K_{12} can be extracted by the following equation [27] for meeting the requirement of the matrix [$\boldsymbol{M}$]:

$$K_{12} = \pm \frac{f_{p2}^2 - f_{p1}^2}{f_{p2}^2 + f_{p1}^2} \tag{2}$$

where f_{p1} and f_{p2} represent the lower and higher split resonant frequencies, respectively. The Q_e can be extracted and attained by

$$Q_e = \frac{f_0}{f_{\pm 90^\circ}} \tag{3}$$

where f_0 and $f_{\pm 90^\circ}$ denote the central frequency and the ±90° bandwidth with respect to the absolute phase at f_0, respectively.

In the first step of the proposed design, C_v with the minimum value (C_{vmin}) is defined as the initial state. Once the passband ripple $L_{Ar} = 0.02$ dB is chosen, the parameters in [$\boldsymbol{M}$] can be determined by using the classic coupling theory [27] of the filter synthesis (described as below) according to the given specifications. Subsequently, the variation slopes and values of Q_e, K_{12}, and M_{SL} should be carefully investigated by using parameters' study for meeting the requirements of the desired ones, which are discussed in the following three parts.

2.1 Q_e

For a second-order filter, the required Q_e is given by

$$Q_e = f_0 \frac{g_0 g_1}{A} \tag{4}$$

where g_0 and g_1 are the element values of Chebyshev lowpass prototype. To maintain constant ABW across the tuning range of f_0, Q_e should be increased as f_0 shifts upward, and the desired variation slope Q_e/f_0 is g_0g_1/A. Accordingly, the passband performance can be good in the frequency-tuning range.

According to the feeding scheme shown in Fig. 2, where the stubs for S–L coupling in Fig. 1 are neglected because their effect on Q_e is slight. Accordingly, Q_e can be obtained from the equation below

$$Q_e = \frac{\omega_0}{2Y_0} \frac{\partial \operatorname{Im}[Y_{in}]}{\partial \omega}\Big|_{\omega = \omega_0} \tag{5a}$$

where

$$Y_{in} = \frac{j\omega C_2 Y_r}{j\omega C_2 + Y_r} \tag{5b}$$

$$Y_r = \frac{jY[\omega Y(C_1 + C_v)(1 - \tan\theta_1 \tan\theta_2)}{(Y - \omega C_1 \tan\theta_1)(Y - \omega C_v \tan\theta_2)} \\ +(\tan\theta_1 + \tan\theta_2)(Y^2 - \omega C_1 C_v)] \tag{5c}$$

From (5), it can be found that Q_e is mainly controlled by C_2, Y, $u = \theta_1/(\theta_1 + \theta_2)$ and C_1, where Y is the characteristic admittance of the resonator, which is determined by the width W_1 of the employed resonator. As a result, Q_e can be the function of these parameters

$$Q_e = f(C_2, W_1, u, C_1) \tag{6}$$

According to the parameters' study shown in Fig. 3 (the variation of frequency in horizontal axis results from the change of C_v, i.e. the resonant frequency of the resonator in Fig. 2 is changed by tuning the value of C_v, where $C_{vmin} = 1$ pF and $C_{vmax} = 8$ pF are used), C_2 affects the value of Q_e and has rare effect on the variation slope of Q_e. As shown in Fig. 3*b*, as W_1 increases, its effect on Q_e becomes slight, especially when $W_1 \geq 0.5$ mm. Both u and C_1 have influence on the Q_e's value and variation slope. It is obvious that the effect of C_1 is much more significant than that of u, as can be seen from Figs. 3*c* and *d*. Accordingly, the incorporation of C_1 is significant for making the value of Q_e close to the desired one in a wide-frequency range, resulting in the broadening of frequency-tuning range of the passband with constant ABW, as compared with the design [24].

2.2 K_{12}

To design a second-order filter, the inter-stage coupling K_{12} is given by

$$K_{12} = \frac{A}{f_0\sqrt{g_1 g_2}} \tag{7}$$

In this design, a mixed electric and magnetic coupling scheme based on the coupling region with length L_1, combining the effect of C_1, is investigated to achieve the constant ABW in a wide-frequency range.

As can be found from the coupling structure in Fig. 1, K_{12} contains two different couplings, i.e. electric coupling (K_e) and magnetic coupling (K_m). To obtain the two couplings, the normalised voltage and current at fundamental resonance are employed, as in Fig. 4. According to the transmission line theory, the normalised voltage and current can be expressed as

$$V_i(x) = \cos\beta_i x \tag{8a}$$

$$I_i(x) = \sin\beta_i x \tag{8b}$$

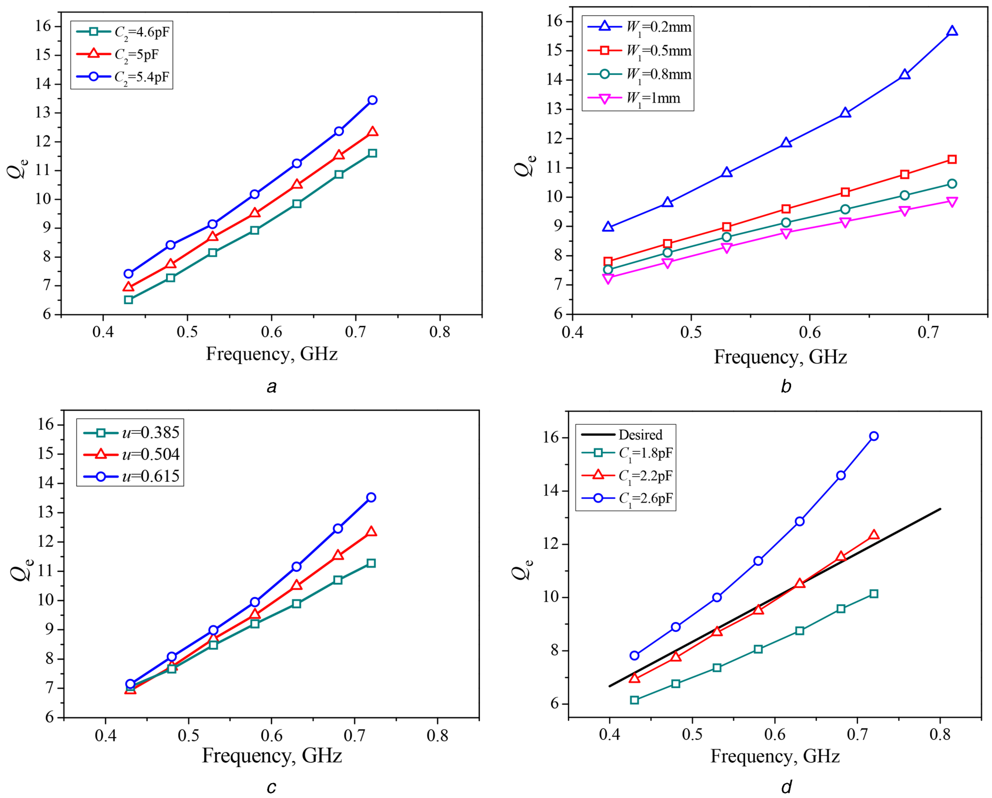

Fig. 3 *Extracted Q_es against different parameters (the parameters $C_2 = 5$ pF, $W_1 = 0.5$ mm, $u = 0.504$, and $C_1 = 2.2$ pF are used. When one parameter is changed, other parameters are fixed as these values)*
(a) Change C_2, ***(b)*** Change W_1, ***(c)*** Change u, ***(d)*** Change C_1

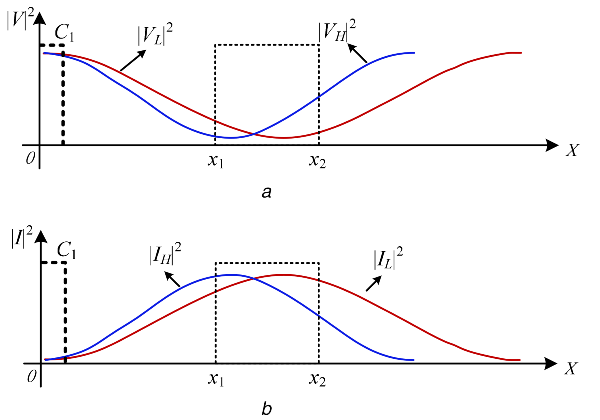

Fig. 4 *Normalised voltage and current at low and high frequencies for the employed tunable λ/2 resonator*
(a) Voltage (electric coupling), ***(b)*** Current (magnetic coupling)

where β_i is the propagation constant and $i = L$ or H. The electric and magnetic coupling coefficients K_e and K_m can be calculated by

$$|K_{e,\,i}| = p \times \int_{x_1}^{x_2} |V_i|^2 \,\mathrm{d}x \tag{9a}$$

$$|K_{m,\,i}| = p \times \int_{x_1}^{x_2} |I_i|^2 \,\mathrm{d}x \tag{9b}$$

where p is a positive constant. Subscripts L and H represent the lower and higher-frequency states, respectively.

According to (9a) and (9b), K_m and K_e can be seen as the areas between the respective curves and x-axis (from x_1 to x_2) in Fig. 4. It can be found that the area of K_m is larger than that of K_e, i.e. the magnetic coupling is dominated. As the coupling region (from x_1 to x_2) is chosen, the variation trends of K_m and K_e can be obtained, namely [24]

$$|K_{e,\,L}| < |K_{e,\,H}| \tag{10a}$$

$$|K_{m,\,L}| > |K_{m,\,H}| \tag{10b}$$

Thus K_{12} can be obtained as

$$|K_{12}| = |K_m| - |K_e| \tag{11}$$

From (10) and (11), we can find K_{12} decreases as f_0 shifts upward, conforming to the condition of constant ABW.

In the proposed filter structure, K_{12} mainly depends on the coupling region with length L_1. Thus, it is controlled by the parameters L_1 (coupling region), d_1 (coupling gap between the two resonators), C_1 and W_1. Moreover, then it can be expressed as

$$K_{12} = f(L_1, d_1, W_1, C_1) \tag{12}$$

Fig. 5 shows these parameters' study. As expected, L_1 has significant effect on the K_{12}'s value and variation slope. In this design, d_1 mainly controls the value of K_{12} and rarely affects the variation slope of K_{12}. On the contrary, W_1 mainly controls the variation slope of K_{12} when $W_1 \geq 0.5$ mm and has slight effect on the value of K_{12}. Meanwhile, C_1 has slight effect on K_{12} including the value and variation slope, as compared with other parameters. As a result, C_1 possesses the ability of fine tuning K_{12} once the dominate parameters such as L_1 and d_1 are determined, so that K_{12} can be further close to the desired one in a wide-frequency range, as in Fig. 5*d*.

According to the above discussion of Sections 2.1 and 2.2, the separate controlling of Q_e and K_{12} can be obtained in the wide-frequency-tuning range. In this design, C_1 acts as a dominate parameter for controlling Q_e while has slight effect on the value of K_{12}. Meanwhile, there is a common point that when $W_1 \geq 0.5$ mm,

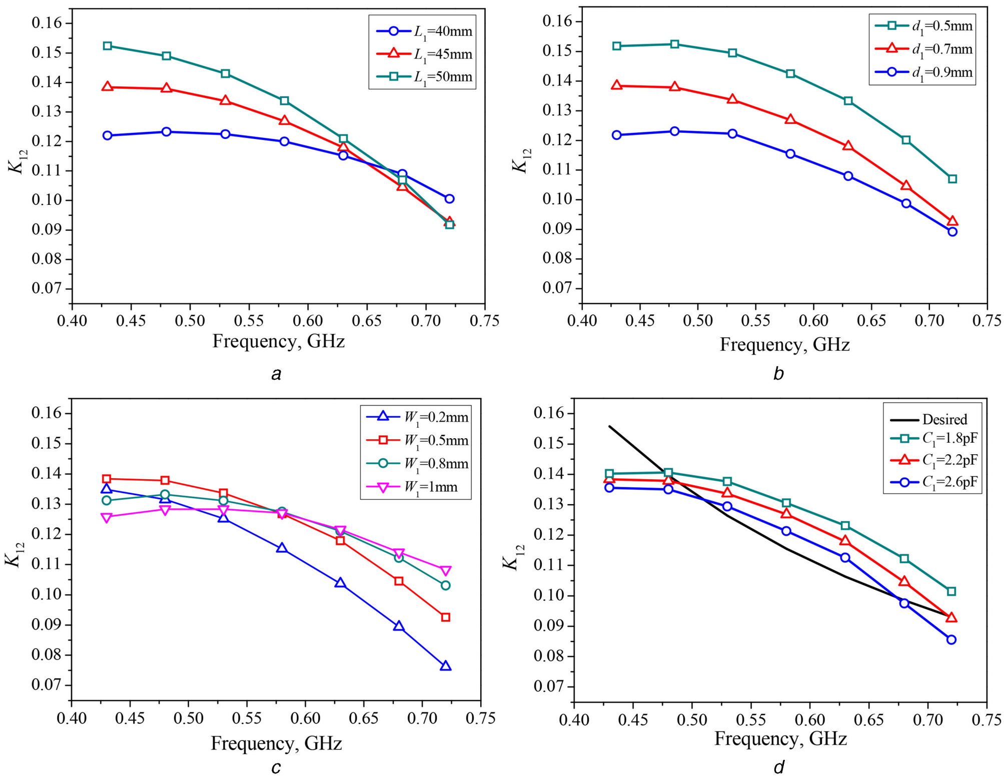

Fig. 5 *Extracted K_{12} against different parameters (the parameters L_1 = 45 mm, d_1 = 0.7 mm, W_1 = 0.5 mm, and C_1 = 2.2 pF are used. When one parameter is changed, other parameters are fixed as these values)*
(a) Change L_1, ***(b)*** Change d_1, ***(c)*** Change W_1, ***(d)*** Change C_1

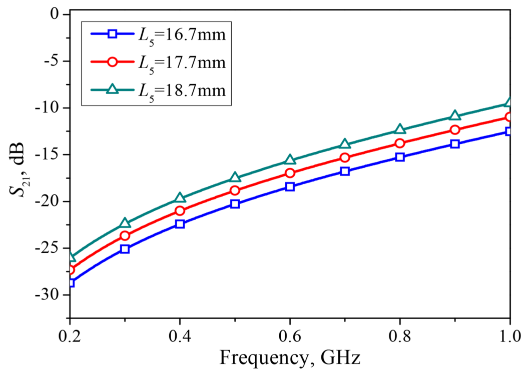

Fig. 6 *Simulated S_{21} of the S–L coupling*

it has only slight effect on both the value of Q_e and the variation slope of K_{12}. Thus, $W_1 = 0.5$ mm is determined in the filter design. There are independent parameters, i.e. C_2 and u for Q_e and L_1 and d_1 for K_{12}, which can be used to independently tune Q_e and K_{12} for meeting the requirement. As a result, the design procedure of the proposed tunable filter is simplified. Accordingly, by properly choosing their values, a wideband tunable BPF with constant ABW can be realised.

2.3 Implementation of self-adaptive TZs

It is well known that the S–L coupling [M_{SL} in (1)] is used to realise the TZs for improving the selectivity, but how to control the TZs in the tunable BPF is still a challenging issue. In this work, two coupled shunt stubs are employed to realise electrically dominated S–L coupling, so that M_{SL} is negative, while M_{S1}/M_{2L}, and M_{12} have opposite sign.

To investigate the improvement of selectivity by the S–L coupling, the coupling matrix simulation software (MATLAB) is employed to calculate the corresponding frequency responses (*S*-parameters). By substituting the extracted Q_e and K_{12} (meeting the requirement of the constant ABW mentioned above) under different f_0 into (1), the desired elements (M_{S1}, M_{12}, and M_{2L}) in the coupling matrix [***M***] can be obtained. Subsequently, the desired S–L coupling M_{SL} in [***M***] can be calculated using MATLAB under different f_0 for meeting the requirements of two TZs at $f_0 \pm 150$ MHz. Hence, the desired variation of M_{SL} which can realise the self-adaptiveness of the TZs along the tunable passband can be obtained. Accordingly, the S–L coupling strength versus frequency should be investigated.

To extract M_{SL}, C_2 in Fig. 1 is set as a very small value (e.g. 0.01 pF), so that the input/output port is isolated from the resonator [28], resulting in a single transmission path (M_{SL}) for the proposed filter. By simulation, the S–L coupling level (S_{21}, dB) can be obtained as shown in Fig. 6. By converting S_{21} in dB to a linear format and then substituting the linear S_{21} at different frequencies in Fig. 6 into (13), M_{SL} at different frequencies can be calculated

$$M_{SL} = \frac{1 - \sqrt{1 - |S_{21}|^2}}{|S_{21}|} \tag{13}$$

where $|S_{21}|$ is in linear format. The calculated coupling matrix $\boldsymbol{M}_1$ at the initial state ($C_v = C_{vmin}$) is obtained as follows:

$$\boldsymbol{M}_1 = \begin{array}{c} \\ S \\ 1 \\ 2 \\ L \end{array} \begin{array}{cccc} S & 1 & 2 & L \\ \hline \end{array}$$

$$\boldsymbol{M}_1 = \begin{array}{c|cccc} & S & 1 & 2 & L \\ \hline S & 0 & 0.682 & 0 & -0.072 \\ 1 & 0.682 & 0 & 0.531 & 0 \\ 2 & 0 & 0.531 & 0 & 0.682 \\ L & -0.072 & 0 & 0.682 & 0 \end{array} \tag{14}$$

By studying the parameters of the coupled stubs, the variation of M_{SL} is achieved, as in Fig. 7. M_{SL} can be tuned by adjusting the coupling between the stubs (i.e. L_5 and d_2 in Fig. 1) to approach the desired values, while the tunable passband keeps almost the same. As a result, two self-adaptive TZs are built for enhancing the selectivity across the frequency-tuning range effectively.

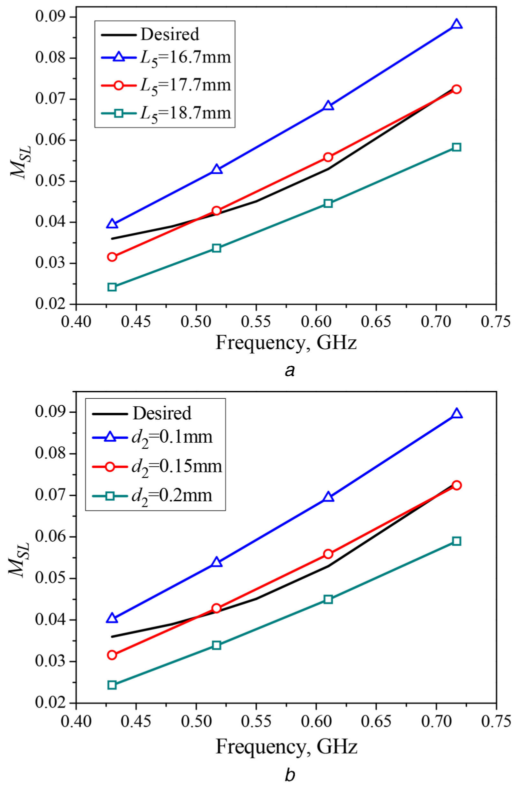

Fig. 7 *Desired and simulated M_{SL}*
(a) Change L_5 when $d_2 = 0.15$ mm, ***(b)*** Change d_2 when $L_5 = 17.7$ mm

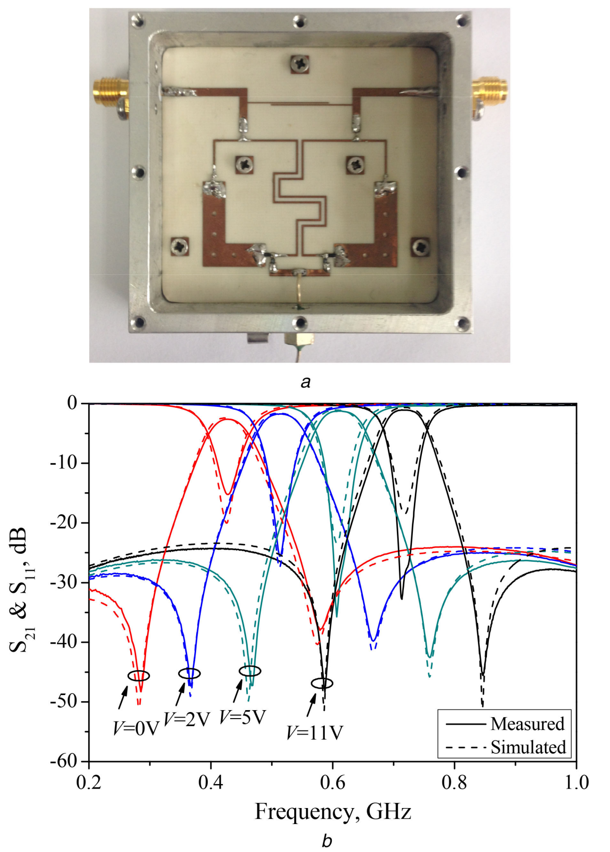

Fig. 8 *Photograph of the fabricated tunable filter for verification*
(a) Photograph of the fabricated tunable BPF, ***(b)*** Measured and simulated *S*-parameters of the proposed tunable BPF

3 Filter design and experimental demonstration

The demonstrated filter is fabricated on the substrate of Rogers RO4003C with a dielectric constant $\varepsilon_r = 3.38$ and a thickness $h =$

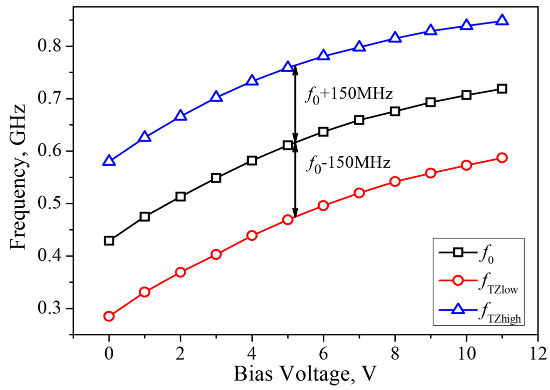

Fig. 9 *Measured f_0 and two TZs frequencies (f_{TZlow} and f_{TZhigh})*

32 mil. The varactor diodes JDV2S71E from Toshiba are used. The DC bias voltage V for the varactor diode is 11–0V, resulting in the corresponding value of C_v changes from 1 to 8 pF. The simulation and experiment are conducted by using high-frequency structure simulator software and Agilent E8363C network analyser, respectively. The design procedures are as follows:

(i) Calculating the desired values of Q_e and K_{12} according to (4) and (7), respectively.
(ii) On the basis of (6) for Q_e and (12) for K_{12}, the extracted values can be close to the desired ones by using correlative parameter studies.
(iii) Substituting the extracted Q_e and K_{12} under different frequencies into (1), and using the coupling matrix [$\boldsymbol{M}$] to calculate the desired values of M_{SL} under different frequencies.
(iv) Studying the key parameters L_5 and d_2 of S–L coupling, the extracted values of M_{SL} under different frequencies can be close to the desired ones. Accordingly, two TZs located at $f_0 \pm 150$ MHz can be obtained across the frequency-tuning range of the passband.

After optimisation, the physical parameters of the filter are determined as $L_1 = 44$ mm, $L_2 = 12.9$ mm, $L_3 = 13.1$ mm, $L_4 = 5$ mm, $L_5 = 17.7$ mm, $W_1 = 0.5$ mm, $W_2 = 0.3$ mm, $d_1 = 0.7$ mm, $d_2 = 0.15$ mm, $C_1 = 2.2$ pF, and $C_2 = 5$ pF. The circuit size is around $0.16\lambda_g \times 0.14\lambda_g$, where λ_g is the guided wavelength at lowest-frequency passband. Fig. 8*a* shows the photograph of the fabricated tunable filter for verification.

In the tunable filter design, the fractional frequency-tuning range is used to evaluate the tunability of the filter. It is generally defined as

$$R_f = \frac{f_{oh} - f_{ol}}{(f_{oh} + f_{ol})/2} \tag{15}$$

where f_{0l} and f_{0h} mean the lowest and highest passband frequencies in the tuning range. Fig. 8*b* shows the simulated and measured results of the proposed filter. The passband frequency can be tuned from 0.72 to 0.43 GHz, corresponding to a fractional tuning range of 50.4%, as the bias voltage V of the varactor diode varies from 11 to 0 V. The measured insertion loss varies from 1.34 to 2.92 dB and the 3 dB ABW is within 75 ± 4 MHz across the frequency-tuning range. Generally, the parasitic resistance R of the varactor diode increases as V is decreased. In this process of frequency decreasing, the unloaded Q value of the employed resonator becomes worst. Accordingly, the two return loss (RL) poles become closer gradually, and even overlapped. As can be seen from Fig. 8*b*, the passband performance including RL and IL is acceptable at every tuning state. As expected, two symmetrical TZs in the lower and higher stopbands are self-adaptive as the passband frequency is tuned, and the distance from the centre frequency to TZs is always constant at 150 MHz across the entire tunable range, as shown in Fig. 9.

Fig. 10*a* plots the output power against the input power of the filter with a bias voltage of 2 V under two-tone test with spacing of

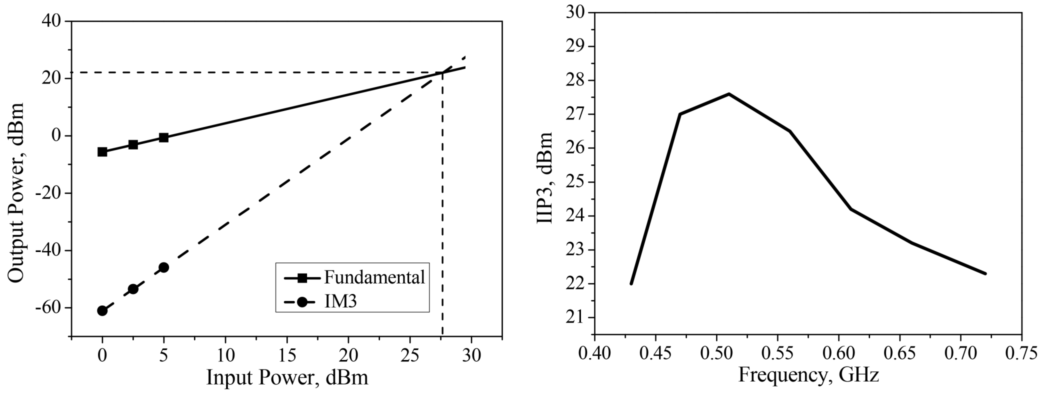

a b

Fig. 10 *Output power against the input power of the filter*
(a) Measurement output power of fundamental signal and 3rd order intermodulation (IM3) of the proposed tunable BPF under a bias voltage of 2 V and two-tone test with separation of 1 MHz, ***(b)*** Measured IIP3 as f_0 varies

Table 1 Comparison with previous tunable filters with constant ABW

Ref.	Implement technology	Tuning range	Filter order/ varactor number	IL, dB	ABW, MHz	IIP3, dBm	Numbers of TZs/self-adaptiveness	Size ($\lambda_g \times \lambda_g$)
[21]	Microstrip	1.1–1.88 GHz (52.3%)	3/3	4.3 − 6.8	90 ± 8	10.8 − 15.8	1/no	0.2 × 0.22
[22]	Microstrip	0.95–1.55 GHz (48.0%)	2/3	2.4 − 2.8	nearly 120	×	1/no	0.28 × 0.23
[23]	Microstrip	0.92–1.03 GHz (11.3%)	2/6	0.16 − 1.41	23.8 ± 0.3	×	0/no	0.2 × 0.17
[24]	Microstrip	0.65–0.96 GHz (38.5%)	2/2	1.2 − 1.5	80 ± 3.5	13	2/no	0.12 × 0.12
		0.63–0.93 GHz (38.5%)	2/2	1.6 − 2.0	60 ± 3	13	2/no	0.12 × 0.12
[25]	Microstrip	0.78–1.36 GHz (54.2%)	2/2	1.68 − 2.9	103 ± 6	×	4/no	0.33 × 0.33
[26]	Microstrip	1.7–2.7 GHz (45.5%)	2/7	3.8 − 4.9	nearly 110	×	2/yes	0.12 × 0.07
[29]	CPW	1.87–2.37 GHz (23.6%)	2/2	1.48 − 1.58	410 ± 10	×	1/no	0.75 × 0.3
this work	Microstrip	0.43–0.72 GHz (50.4%)	2/2	1.34 − 2.92	75 ± 4	22-27.6	2/yes	0.16 × 0.14

1 MHz. Fig. 10*b* shows the measured input third-order intercept point (IIP3) in the frequency-tuning range. It can be seen that the filter exhibits an IIP3 of better than 22 dBm throughout the entire filter tuning range. The IIP3 of tunable filter highly depends on the non-linearity of the employed varactor diode. The IIP3 of the proposed design is higher than those of the previous designs with constant ABW in [21, 24]. This is because the adopted diodes are different.

Table 1 summarises the comparison of the proposed design with constant ABW. It is obvious that microstrip tunable filters possess wider frequency-tuning range of the passband and smaller circuit size, as compared with the coplanar waveguide (CPW) [29] design. Although the TZs are discussed in some microstrip tunable filters [24, 25], their self-adaptiveness as the passband changes is rarely mentioned. In [26], a tunable S–L coupling realised by extra varactor diodes is used to generate two self-adaptive TZs close to the passband. However, too many varactor diodes are used, leading to the increase of IL (about 3.8–4.9 dB). As can be observed from Table 1, the proposed filter has competitive performance such as high selectivity resulting from two self-adaptive TZs, wide-frequency-tuning range, and low passband IL, as compared with most previous designs.

4 Conclusion

In this paper, a wideband tunable BPF with constant ABW and continuously high selectivity has been presented. The frequency-dependent S–L coupling is introduced in the tunable filter design for the first time, so that the two generated TZs are self-adaptive. Moreover then, the separations between the passband centre frequency and two TZs always keep the same across the whole frequency-tuning range. Meanwhile, the incorporated S–L coupling hardly affects the passband performance. The constant ABW in the tuning process of the passband can be obtained by investigating Q_e and K_{12}. The design procedures of the proposed design are discussed and given in detail. The simulated and measured results of the demonstration filter are presented, showing good agreement. The good performance makes the filter more attractive in the practical and industrial applications.

5 Acknowledgments

This work was supported by the Natural Science Foundation of Jiangsu province under grant BK20161281, by Science-Technology Programs of Nantong under grants CP22014005 and AA2014013, by the Graduate Research and Innovation Plan Project of the Universities of Jiangsu Province under grant KYLX16_0971, and by the Nantong Application Research Technology Programme under grant GY12015021.

6 References

[1] Cheng, C.C., Rebeiz, G.M.: 'High-Q 4–6 GHz suspended stripline RF MEMS tunable filter with bandwidth control', *IEEE Trans. Microw. Theory Tech.*, 2011, **59**, (10), pp. 2469–2476

[2] Pranonsatit, S., Holmes, A.S., Lucyszyn, S.: 'Microwave modelling of radio frequency microelectromechanical rotary switches', *IET Microw. Antenna Propag.*, 2010, **5**, (3), pp. 255–261

[3] Somjit, N., Oberhammer, J.: 'Design approach for return-loss optimisation of multi-stage millimetre-wave microelectromechanical systems dielectric-block phase shifters', *IET Microw. Antenna Propag.*, 2012, **6**, (13), pp. 1429–1436

[4] Ishak, W.S., Chang, K.W.: 'Tunable microwave resonators using magnetostatic wave in YIG films', *IEEE Trans. Microw. Theory Tech.*, 1986, **34**, (12), pp. 1383–1393

[5] Yun, T.Y., Chang, K.: 'Piezoelectric-transducer-controlled tunable microwave circuits', *IEEE Trans. Microw. Theory Tech.*, 2002, **50**, (5), pp. 1303–1310

[6] Zhu, H., Abbosh, A.: 'Compact tunable bandpass filter with wide tuning range of centre frequency and bandwidth using coupled lines and short-ended stubs', *IET Microw. Antenna Propag.*, 2016, **10**, (8), pp. 863–870

[7] Hong, J.S.: 'Reconfigurable planar filters', *IEEE Microw. Mag.*, 2009, **10**, (6), pp. 73–83

[8] Hunter, I.C., Rhodes, J.D.: 'Electronically tunable microwave bandpass filters', *IEEE Trans. Microw. Theory Tech.*, 1982, **MTT-30**, (9), pp. 1354–1367

[9] Zhang, X.Y., Chan, C.H., Xue, Q., *et al.*: 'RF tunable bandstop filters with constant bandwidth based on a doublet configuration', *IEEE Trans. Ind. Electron.*, 2011, **59**, (2), pp. 1257–1265

[10] Mao, J., Che, W., Ma, Y., *et al.*: 'Tunable differential-mode bandpass filters with wide tuning range and high common-mode suppression', *IET Microw. Antenna Propag.*, 2014, **8**, (6), pp. 437–444
[11] Wong, P.W., Hunter, I.C.: 'Electronically tunable filters', *IEEE Microw. Mag.*, 2009, **10**, (6), pp. 46–54
[12] Beukman, T.S., Geschke, R.H.: 'A tune-all wideband filter based on perturbed ring-resonators', *IEEE Microw. Wirel. Compon. Lett.*, 2013, **23**, (3), pp. 131–133
[13] Sun, J.S., Kaneda, N., Baeyens, Y., *et al.*: 'Multilayer planar tunable filter with very wide tuning bandwidth', *IEEE Trans. Microw. Theory Tech.*, 2011, **59**, (11), pp. 2864–2871
[14] Cho, Y.H., Rebeiz, G.M.: 'Two- and four-pole tunable 0.7–1.1 GHz bandpass-to-bandstop filters with bandwidth control', *IEEE Trans. Microw. Theory Tech.*, 2014, **62**, (3), pp. 457–463
[15] Cho, Y.H., Rebeiz, G.M.: 'Tunable 4-pole noncontiguous 0.7–2.1 GHz bandpass filters based on dual zero-value couplings', *IEEE Trans. Microw. Theory Tech.*, 2015, **63**, (5), pp. 1579–1586
[16] Zhu, H., Abbosh, A.: 'Tunable band-pass filter with wide stopband and high selectivity using centre-loaded coupled structure', *IET Microw. Antenna Propag.*, 2015, **9**, (13), pp. 1371–1375
[17] Tang, C.W., Chen, W.C.: 'A compact tunable notch filter with wide constant absolute bandwidth', *IEEE Microw. Wirel. Compon. Lett.*, 2015, **25**, (3), pp. 151–153
[18] Chen, J.X., Ma, Y.L., Cai, J., *et al.*: 'Novel frequency-agile bandpass filter with wide tuning range and spurious suppression', *IEEE Trans. Ind. Electron.*, 2015, **62**, (10), pp. 6428–6435
[19] Mao, J.R., Choi, W.W., Tam, K.W., *et al.*: 'Tunable bandpass filter design based on external quality factor tuning and multiple mode resonators for wideband applications', *IEEE Trans. Microw. Theory Tech.*, 2013, **61**, (7), pp. 2574–2584
[20] Athukorala, L., Budimir, D.: 'Compact second-order highly linear varactor-tuned dual-mode filters with constant bandwidth', *IEEE Trans. Microw. Theory Tech.*, 2011, **59**, (9), pp. 2214–2220
[21] Zhao, Z.Y., Chen, J., Yang, L., *et al.*: 'Three-pole tunable filters with constant bandwidth using mixed combline and split-ring resonators', *IEEE Microw. Wirel. Compon. Lett.*, 2014, **24**, (10), pp. 671–673
[22] Tang, C.W., Tseng, C.T., Chang, S.C.: 'Design of the compact tunable filter with modified coupled lines', *IEEE Trans. Compon. Packag. Manuf. Technol.*, 2014, **4**, (11), pp. 1815–1821
[23] Suo, G., Guo, X., Cao, B., *et al.*: 'Superconducting varactor tunable filter with constant bandwidth using coupling line', *IEEE Microw. Wirel. Compon. Lett.*, 2014, **24**, (9), pp. 628–630
[24] Zhang, X.Y., Xue, Q., Chan, C.H., *et al.*: 'Low-loss frequency-agile bandpass filters with controllable bandwidth and suppressed second harmonic', *IEEE Trans. Microw. Theory Tech.*, 2010, **58**, (6), pp. 1557–1564
[25] Ge, C., Zhu, X.W.: 'Highly-selective tunable bandpass filter with two-path mixed coupling', *IEEE Microw. Wirel. Compon. Lett.*, 2014, **24**, (7), pp. 451–453
[26] Chi, P.L., Yang, T., Tsai, T.Y.: 'A fully tunable two-pole bandpass filter', *IEEE Microw. Wirel. Compon. Lett.*, 2015, **25**, (5), pp. 292–294
[27] Hong, J.S., Lancaster, M.J.: '*Microwave filters for RF/microwave applications*' (Wiley, New York, 2011)
[28] Cameron, R.J.: 'Advanced coupling matrix synthesis techniques for microwave filters', *IEEE Trans. Microw. Theory Tech.*, 2003, **51**, (1), pp. 1–10
[29] Chen, Z.H., Zhang, S.X., Chu, Q.X.: 'A novel reconfigurable bandpass filter with compensable coupling based on microstrip-to-CPW structure'. Asia-Pacific Microwave Conf. Digest, December 2015, pp. 1–3